Corrosion Inhibition of Aluminum by *Cerumium rubrum* Extract in Hydrochloric Acid Environment

A. S. Fouda[1] · E. E. El-shereafy[2] · A. A. Hathoot[2] · N. M. El-bahrawi[1]

Abstract

The inhibitive action of *Cerumium rubrum* extract against the corrosion of Al in a 1-M HCl environment was examined using conventional electrochemical and chemical methods. The results indicate that the extract exhibited excellent anticorrosive properties of aluminum in HCl reaching approximately 86.2% at 300 ppm at 318 K. It obeys the Langmuir adsorption isotherm. Polarization curves indicate that the extract acts as a mixed-type inhibitor. Moreover, the kinetic and thermodynamic parameters for the corrosion reaction were estimated and debated. The covering film established by the extract was checked by several techniques. All techniques gave similar results.

Keywords Corrosion inhibition · Aluminum · HCl · *Cerumium rubrum* · EFM · EIS

1 Introduction

Corrosion is a surface phenomenon which occurs naturally when metals have a tendency to revert to their stable nature. Corrosion can be monitored by inhibitors which mainly contain in their bulk structure some of heteroatoms which help in diminishing the rate of corrosion based on their strength, nature of the metal and the corrosive solution surrounding the metal, taking into consideration environmental protection. Previously, organic inhibitors were utilized but it was found that they were toxic to humans and microorganisms meaning they were not eco-friendly, so it became very necessary to research and develop corrosives to find very good inhibitors, which have availability, low cost, non-toxic, and can diminish the corrosion rate, by studying the features of the adsorbents and checking them by surface scanning and confirming their protection ability. Because aluminum is easily corroded by the atmosphere, its corrosion potential is high ($= -1.66$ V) and forms as a thin layer on its surface. As a hindrance towards destruction, we want to insulate its surface from any damage, helping to preserve its features

and using time and money to repair aluminum objects. In our study, we have focused our attention on plant extracts as a natural source [1–10], due to their effectiveness in inhibiting corrosion of different metals and because they are a rich source of ingredients which help to diminish the corrosion of metals which is a major industrial problem. Moreover, we have studied iwhether or not there is a biological effect, paying attention to the environment of the metal, as hydrochloric acid, which has been chosen due to it being considered as a pickling liquid which removes scales and impurities, and is used in refining metals and cleaning [8–13]. In the present research, the corrosive solution is 1 M hydrochloric due to it being the most utilized industrial corrosive medium. Hydrochloric acid reacts with Al and vigorously liberates H_2 gas indicating the dissolution of the Al as ween by the naked eye. The choice of Al as the studied metal is due to it having many applications in the varied aspects of life and industry. Al has four main uses: (1) in general products (beverages, packaging food, trays, foils, refrigerators, toasters, smartphones, labtops) [14] due to it being a good conductor [15] of heat, helping in keeping electronic devices from overheating; (2) transportation, being used by NASA spacecraft due to its light weight and strength under pressure; (3) in electrical products (satellite dishes, sound systems), due to its high corrosion resistance [16, 17]; and (4) architecture (in banks and aquatic centers) due to its strong, flexible, and docile properties. The aim of this research is to examine the influence of *Cerumium rubrum* extract (CRE) on Al corrosion

✉ A. S. Fouda
  asfouda@hotmail.com

1 Chemistry Department, Faculty of Science, El-Mansoura University, Mansoura, Egypt

2 Chemistry Department, Faculty of Science, El-Menoufia University, Shebin El-koom, Egypt

using gravimetric, potentiometric polarization (PP), electro-chemical impedance spectroscopy (EIS) and electrochemical frequency modulation (EFM) methods. The surface analysis of Al was performed using atomic force microscope (AFM) and attenuated total refraction infra-red (ATR-IR).

2 Materials and Methods

2.1 Al Specimen Design

Al samples for the chemical methods and surface analysis utilized in this investigation were in the shape of squares, cut by a wire machine to avoid dissimilar angles and distortion of the lattice structure resulting from other utilized methods, with 20 mm length, 20 mm width and 0.2 cm high with a purity of 99.9%. The working electrode for the electro-chemical corrosives had a magnitude of 1×1 cm^2 and was welded with copper wire, enclosed by a glass rod utilizing epoxy, then left for 24 h for good cohesion. The samples were mechanically abraded by various grades of silicon carbide sheets (320–1200) until having the appearance of a mirror, then washed with double-distilled water, and wiped with acetone.

2.2 Experimental Solutions Preparation

The corrosive solution was 1 M of 37% HCl prepared by dilution with double-distilled water and titrated against 1 M Na$_2$CO$_3$. Solutions with or without various doses of CRE stock from 50 to 300 ppm were freshly prepared.

2.3 CRE Procedure

The dehydrated plant was ground into tiny parts of 5 to 10 mm with a cylindrical grinder and extraction occurred utilizing doubled-distilled water. Then, 0.1 kg of the dehydrated plant was added to 250 ml of double-distilled water at 353 K for half an hour, then kept for 24 h and water-filtered by a filter paper utilizing a glass funnel, diluted to 1000 ml by doubled-distilled water and finally preserved in a cooling system in a glass flask closed with a plastic cover [18]

2.4 Chemical Constituents Found in the (CRE) Plant

CRE belongs to the Ceramiaceae family; *Cerumium* is a genus of red algae (or Rhodophyta). It is a large genus with a minimum 15 species in the British Isles. It has been found that the principal constituents are phytol (44.7%) and palmitic acid (25.8%) [19]. In other research, it was found that palmitic acid was the principal fatty acid, and it was estimated that the total acid content was 57.90% and that saturated fatty acids were the major constituents as shown

in Table 1 ($71.61\% \pm 3.08\%$). The total of monounsaturated fatty acids have a ratio from 8.05 to 12.12%, while the total of polyunsaturated fatty acid was 16.28–29.37% [20]. The following components have been found: loss on drying 11.01%, ash 13.83%, organic substance 75.16%, total nitrogen 3.19%, proteins 19.94%, lipids 3.43%, carbohydrates 51.90%, and beta-carotene in liposoluble substances 0.2199 (mg/100 g) [21]. It has been observed that there were contents of 4.95 mg/kg Pb, 0.206 mg/kg Cd, 5.43 mg/kg Cu, and 5.51 mg/kg Zn [22].

Part Use The numerous species of red algae show antimicrobial, antibacterial, and antifungal activity [19], and generate a superior agar. *Ceramium rubrum* is unique in having strong antibiotic characteristics over Gram-positive bacteria, e.g., *Bacillus subtilis*, but no inhibitory effect has been demonstrated against Gram-negative bacteria. There is also high anti-oxidant activity [22].

2.5 Gravimetric Estimations (Weight Loss, WL)

The utilized samples in WL had dimensions of 20 mm $\times$ 20 mm $\times$ 0.2 cm. The samples were abraded one after another with various successions of emery sheets of dissimilar grades from 320 to 1200 grade, dry-cleaned with acetone, and air-dried. The WL corrosive was added in 100 ml 1 M HCl mixtures with and without various doses of the CRE. The ratios of dissolution were assessed utilizing the equation [23]:

$$(CR) = \Delta m / st \tag{1}$$

The reduction of the weight is indicated as Δm, the surface area of the samples exposed to the solution in cm^2 as s, and the dipping time as t. The inhibition efficiency or (protection quality), %IE, and surface coverage, θ, were assessed utilizing the equation:

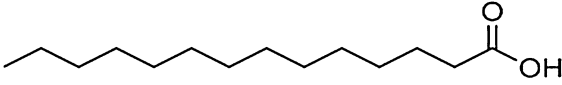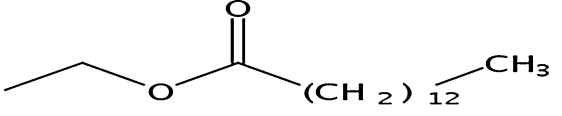$$\%IE = \theta \times 100 = 1 - \left[CR_{inh} / CR_{corr} \right] \times 100 \tag{2}$$
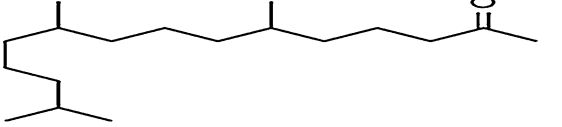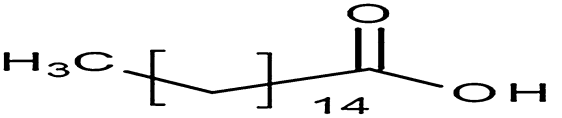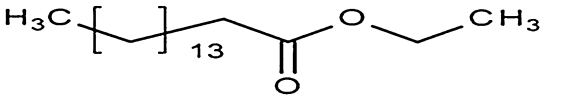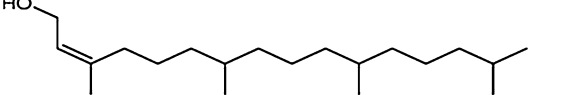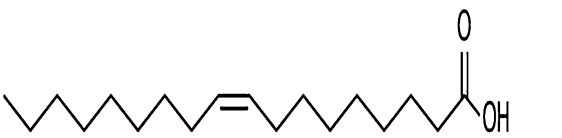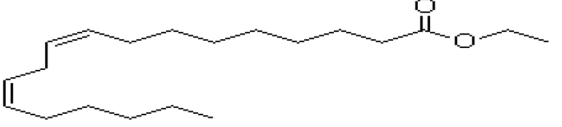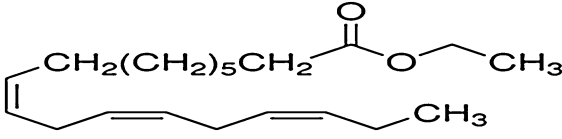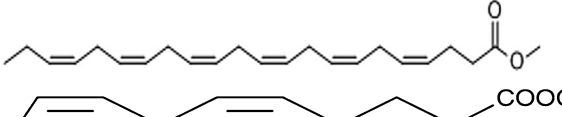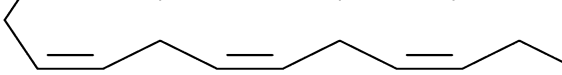
The dissolution ratios of Al with and without CRE are shown as CR_{inh} and CR_{corr}.

2.6 Hydrogen Evolution Method

The same Al samples utilized for the gravimetric method were utilized for the H$_2$ evolution method. Before the corrosive performance, the Al samples were abraded with the selected levels of emery papers beginning from roughest to finest, then treated with acetone and air-dried. The samples were dipped in a 100-ml closed bottle including the prepared solution. H$_2$ gas evolved and was collected through a

Table 1 List of the major phytochemical constituents in CRE

Some of chemical constituents present in CRE	
	Hexadecane [19]
	Myristic acid [19]
	Ethyl myristate [19]
	Hexahydrofarnysl acetone [19]
	Hexadecanoic acid (palmitic acid) [19, 20]
	Ethyl palmitate [19]
	Phytol [19]
	Oleic acid [19]
	Stearic acid [19]
	Ethyl linoleate [19]
	Ethyl linolenate [19]
	DHA methyl ester [19]
	EPA methyl ester [19]

Table 1 (continued)

Some of chemical constituents present in CRE
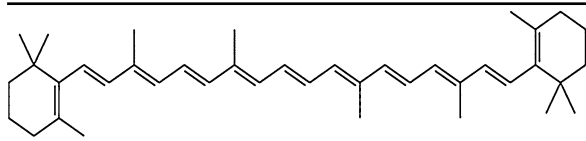
	Beta-carotene [21]

tube connected to a gas burette standing in a beaker filled with water, as reported before [24]. The shift of the volume was caused by air compression. This allowed the estimation of the volume of gas evolved as a function of time. The H_2-evolution was performed with and without the presence of the various doses of the extract. R_B (rate without extract) is V_{H_2} evolution divided by the corresponding time and R_E (rate with extract) is the difference in V_{H_2} without inhibitor and V_{H_2} with extract divided by the corresponding time [25]. The (%IE) was computed utilizing the equation:

$$\%IE = \left[R_B - R_E\right]/\left[R_B\right] \times 100 \tag{3}$$

2.7 Acidification Method

The pH was checked for the six doses of 50, 100, 150, 200, 250 and 300 ppm pre- and post-dipping in the checked solution for 3 h.

The hydrogen ion (H^+) was calculated in each case utilizing the following equation:

$$pH = \log[H] \tag{4}$$

2.7.1 Corrosion Rate

The corrosion rate (CR) of the Al samples was calculated utilizing Eq. 5:

$$CR \left(mol\, dm^{-3}\, cm^{-2}\, h^{-1}\right) = \left[\Delta H^+\right]/At \tag{5}$$

where $[\Delta H^+]$ is the difference between the initial and final concentrations of H^+, A is the surface area of the sample in cm^2 and t the time in hours.

2.7.2 Inhibition Efficiency and Surface Coverage (θ)

The IE was evaluated using utilizing Eq. 6 [26]:

$$\%IE = \theta \times 100 = \left\{1 - \left[\Delta H^+\right]_{inh}/\left[\Delta H^+\right]_{uninh}\right\} \times 100 \tag{6}$$

where $[\Delta H^+]_{inh}$ and $[\Delta H^+]_{uninh}$ are changes in $[H^+]$ with and without the extract, respectively.

2.8 Potentiodynamic Polarization (PP) Method

Corrosives were achieved in a classic three-electrode cell utilizing a counter electrode, a reference electrode and a working electrode. The working electrode was made from the same Al sheet used in the chemical method, the area of the exposed surface positions was 1 cm^2, and before any corrosive, the electrode surface was treated in the same procedure as in the gravimetric method. Then, the electrode was dipped in the corrosive solution at the open-circuit potential (OCP) for ½ h until a steady state was obtained. Computations were taken as a function of current densities, the %IE for each dose of the CRE was estimated using the equation [27]:

$$\%IE = \theta \times 100 = 1 - \left[i_{inh}/i_{corr}\right] \times 100 \tag{7}$$

Here, i_{corr} and i_{inh} are the dissolution current densities estimated from Tafel slopes without and with CRE doses.

2.9 Alternating Current Impedance Spectra (EIS) Method

The EIS was processed utilizing the same cell order as mentioned before in PP. EIS estimations were proved by utilizing AC signals with an amplitude of 10 mV peaks at the OCP in the frequency range of 100 kHz to 0.1 Hz. All the impedance results conformed to the convenient equivalent circuit utilizing the software of Gamry Echem Analyst, and the protection quality, %IE, was taken as a function of the estimated R_{ct} [28].

2.10 Electrochemical Frequency Modulation (EFM) Method

Stratifying signals with amplitude 10 mV to 2 and 5 Hz is the way to proceed with the EFM method which is considered as a quick, non-ruinous and dependable electrochemical method. The current density, (i_{corr}), the Tafel slopes, (β_c) and β_a), and the causality factors, (CF-2 and CF-3), can be immediately estimated from the higher peaks [29]. The apparatus utilized in EFM examinations was the Gamry Potentiostat/Galvanostat/ZRA (PCI4-G750). Gamry software comprises

DC105 software for DC corrosion, EIS300 software for electrochemical impedance spectroscopy, and EFM140 for electrochemical frequency modulation estimations, as well as a computer for data collection. Echem analyst version 5.5 software was utilized for scheming, figuring and fitting the data.

2.11 Surface Inspection

2.11.1 ATR-FTIR and UV/Visible Spectral Analysis

ATR-FTIR determination gives a qualitative characterization to the extract adsorption on the Al surface [30]. The Al coupons inserted in the corrosive solution within 24 h post-dipping duration with and without the CRE were inspected by a Thermo Fisher Scientific IS-10 FT-IR and ATR, in order to examine the features of the film covering the surface of the samples. The corrosive solution containing CRE after insertion of the Al samples for 24 h was measured on a PG UV/VIS Spectrophotometer T80+; pure CRE was also treated by the same apparatus.

2.11.2 AFM Analysis

The AFM technique was used to investigate the morphological characteristics of the Al surface in the corrosive solution without and with CRE. The coupons of Al were treated like the gravimetric method and inserted in the corrosive solution without and with 300 ppm of the CRE for 24 h at 298 K. After this time, the coupons were removed, carefully rinsed with double-distilled water and dried by filter paper [31]. Then, the surface examination was investigated utilizing AFM performed in contact mode utilizing a silicon nitride probe (model MLCT; Bruker). Proscan 1.8 software was used to control the scan parameters and IP 2.1 software for image analysis. Scan parameters: scan area: -10×10 μm^2, scan rate: 1 Hz. Number of data points: the measured area divided into 256 lines and every line divided into 256 points. The scanned area was 2 μm per division, and as there are 5 divisions, so it equals 10×10 μm^2.

## 2.12 Assessment the Inhibition of CRE Against Microbial Growth

The CRE was examined for inhibitory action against the bacterial growth of the total bacteria present in the cooling tower of the ammonia plant at the Talkha factory for fertilizers by performing the spore suspension method. The bacteria were cultivated in a plate over nutrient agar, then after growth, several swabs were taken and multiplied in a 1-l measuring flask containing double-distilled water. This was then left for 1:3/2 h before cultivation before pouring from it into a 100-ml flask containing 10 ml of HCl and 30 ml of CRE, then filling it to 100 ml. It was then left

it for ½–1 h. before 2 ml was taken from the solution by syringe and poured over freshly prepared agar solution in several plates and waiting for a maximum of 2 days. All the plates were incubated at 310 K then the colonies were counted using a UVP colony DOC-It apparatus. The plate containing the CRE showed good resistance to the total bacteria, and the same was carried out for pure CRE only and gave the same outcome, which means that the CRE is resistant for this bacteria and for the bare solution.

3 Results

3.1 Weight Loss (WL) Estimations

Weight Loss (WL) of the Al samples was registered periodically, at 30, 60, 90, 120, 150 and 180 min at separate temperatures, 298, 303, 308, 313 and 318 K; the WL graph at 298 K is shown in Fig. 1. The %IEs at various temperatures are set out in Table 2. The impact of temperature on %IE is shown in Fig. 2. The results indicate that the insertion of CRE diminishes the Al ratios of dissolution in 1 M HCl solution. The %IE was monitored and increased with the increase of the dose of plant extract, as seen in Table 2. This referred to the adsorption of extract particles on the Al surface. These adsorbents diminish the Al destruction by passivation of the corrosion sites as the dose of the extract increases, so increasing the quality.
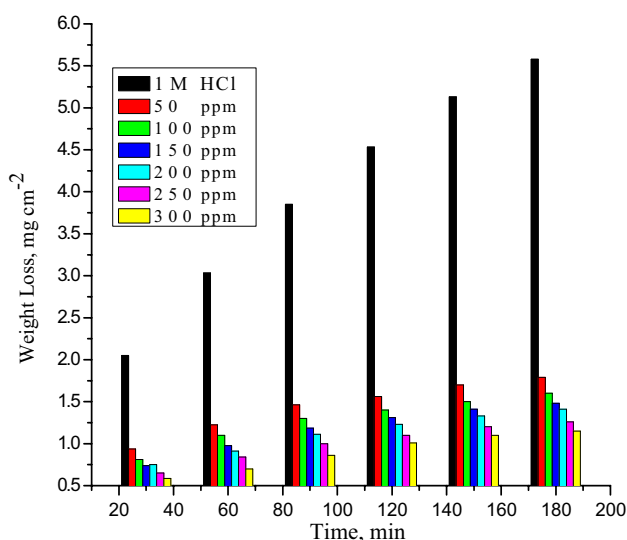
Fig. 1 Weight loss against time for Al in 1 M HCl (corrosive solution) with and without various doses of CRE at 298 K

Table 2 Effect of addition of various doses of CRE on the (Θ) and (%IE) at different temperatures

Temp. (K)	Conc., (ppm)	CRE	
		θ	% IE
298	50	0.658	65.8
	100	0.684	68.4
	150	0.710	71.0
	200	0.737	73.7
	250	0.763	76.3
	300	0.789	78.9
303	50	0.654	65.4
	100	0.709	70.9
	150	0.727	72.7
	200	0.745	74.5
	250	0.764	76.4
	300	0.800	80.0
308	50	0.680	68.0
	100	0.707	70.7
	150	0.747	74.7
	200	0.760	76.0
	250	0.787	78.7
	300	0.813	81.3
313	50	0.701	70.1
	100	0.735	73.5
	150	0.768	76.8
	200	0.793	79.3
	250	0.810	81.0
	300	0.859	85.9
318	50	0.717	71.7
	100	0.748	74.8
	150	0.771	77.1
	200	0.801	80.1
	250	0.817	81.7
	300	0.862	86.2

3.1.1 Adsorption Isotherms

The implementation of adsorption isotherms was estimated to focus on whether the adsorption behavior is chemical or physical [32]. The estimates of θ were gained from the WL method and is a function of CRE doses which were then graphed to fit the most appropriate form of adsorption to compute the adsorption isotherms [33]. To identify the adsorption model, various isotherms were tried (Frumkin, Langmuir, Temkin, Freundlich). The Langmuir adsorption isotherm (Fig. 3) proved the best, and provides a straight-line graph for the scheme of $C/$ against C [11]:
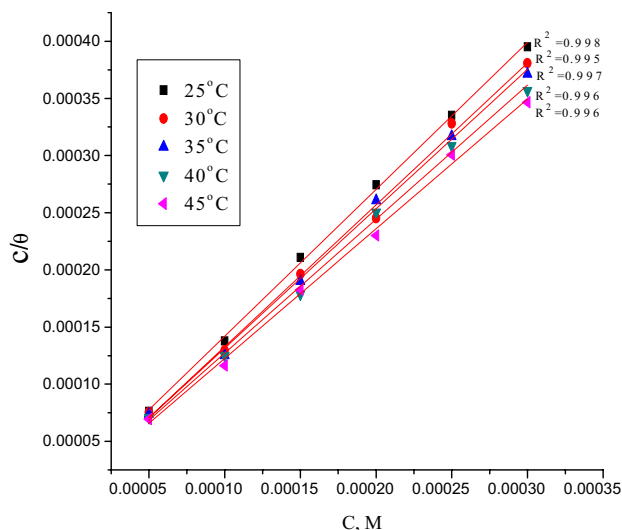
$$C/\theta = 1/K + C \tag{8}$$

where the doses of the extract are expressed as C, and the adsorptive equilibrium constant is K_{ads} which can be computed from the intercept of the variation between the $C/$ and C in Fig. 3 ($\theta = IE/100$). The relationship between K_{ads} and standard free energy expressed as $\left(\Delta G°_{ads}\right)$, can be estimated from Eq. 7, while Fig. 4 explains the variation between log K_{ads} and $1/T$. The slope of this line indicates the value of $\Delta H°_{ads}$ by implementing in Eq. 9

$$K_{ads} = 1/55.5 \exp \left[-\Delta G°_{ads}\right]/RT \tag{9}$$

where R is the universal gas constant, T is the absolute temperature and 55.5 is the molar concentration of water in M^{-1}.

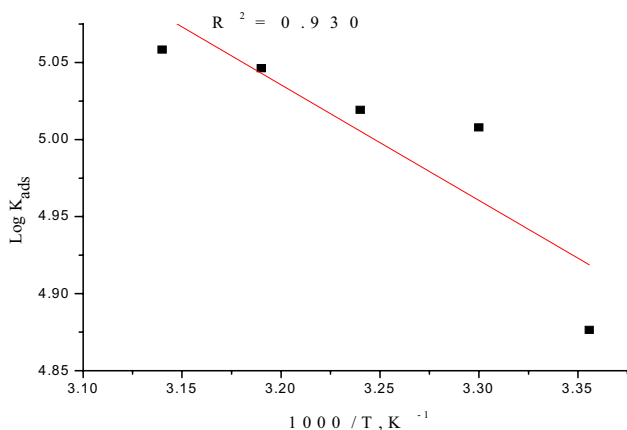The Vant't Hoff equation can be utilized to compute $\Delta H°_{ads}$

$$\log K_{ads} = \Delta H°_{ads}/2.303RT + \text{Constant} \tag{10}$$

Fig. 2 Effect of temperature on %IE utilizing different doses of CRE on the Al surface in 1 M HCl (corrosive solution)
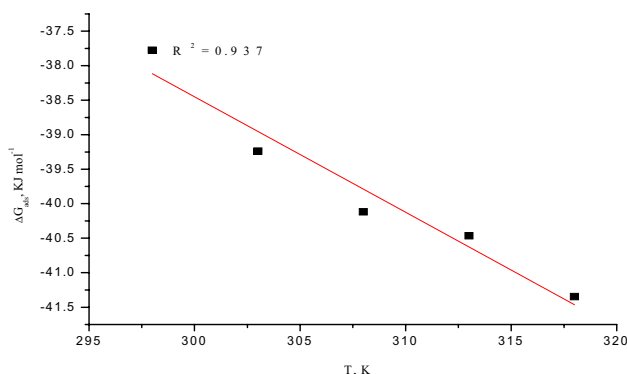
Fig. 3 Langmuir adsorption graph for Al in 1 M HCl (corrosive solution) including different doses of CRE at various temperatures in the range 298–318 K

Fig. 4 Plot of (log K_{ads}) against (1000/T) for the dissolution of Al in 1 M HCl (corrosive solution) + 300 ppm CRE

Fig. 5 Plot of $\Delta G°_{ads}$ versus T for the adsorption of 300 ppm CRE on the Al surface in 1 M HCl (corrosive solution) at different temperatures

Table 3 Adsorption parameters of CRE for the Al surface in 1 M HCl (corrosive solution) generated from the Langmuir adsorption isotherm at different temperatures

Temp. (K)	K_{ads}, (ppm × 10^3)	$-\Delta G°_{ads}$ (kJ mol^{-1})	$\Delta H°_{ads}$ (kJ mol^{-1})	$\Delta S°_{ads}$ (J mol^{-1} K^{-1})
298	75.2	37.8	14.4	126.8
303	104.5	39.2		129.3
308	114.4	40.1		129.5
313	101.8	40.5		130.1
318	111.2	41.3		130.3

Table 4 Kinetic-thermodynamic parameters for Al dissolution with and without different doses of CRE with the 1 M HCl (corrosive solution)

Activation parameters			
Conc. (ppm)	E_a^* (kJ mol^{-1})	ΔH^* (kJ mol^{-1})	$-\Delta S^*$ (J mol^{-1} K^{-1})
Blank	73.2	21.3	106.9
50	54.7	17.5	145.0
100	51.2	17.9	143.4
150	50.2	17.3	148.5
200	43.7	15.6	162.4
250	42.4	16.0	159.7
300	34.1	11.5	194.7

The plot of $\Delta G°_{ads}$ versus T is shown in Fig. 5 and is as reported by the thermodynamic basic Eq. 11

The slope equal to $\Delta S°_{ads}$ can be computed:

$$\Delta G°_{ads} = \Delta H°_{ads} - T\Delta S°_{ads} \tag{11}$$

The negative value of $\Delta G°_{ads}$ refers to the spontaneous adsorption of the extract particles on the surface of the Al. Hence, the value of $\Delta G°_{ads}$ ranged from 37.98 to 41.3 kJ mol^{-1} (Table 3), assisting the suggested chemisorption mechanism. $\Delta G°_{ads}$ value up to -20 kJ mol^{-1} is coherent with physisorption mechanism while that more negative than -40 kJ mol^{-1} assigns chemisorption mechanism [34]. The experimental data fits the utilized adsorption isotherm as the correlation coefficients (R^2) close to 1. The K values raises with raising in temperature Table 3. K value points to the strength between adsorbent and adsorbate [35], its ranges raises with raising temperature, and this confirms the chemical mechanism. An exothermic adsorption process ($\Delta H°_{ads} < 0$) may include either physical adsorption or chemical adsorption or a combination of them, while endothermic process is typical to chemical adsorption. The exothermic adsorption matched from the elucidation of the negative and large estimates of the entropy change ($\Delta S°_{ads}$) in the presence of the considered extract is endothermic ($\Delta S°_{ads} > 0$).

3.1.2 Effect of Temperature (Kinetic–Thermodynamic Parameters)

At various temperatures from 298 to 318 K in the presence of various dosages of CRE, the WL method was achieved. It was found that the rise in temperature is α with CR increasing. In Table 2, the CR of Al without CRE increased sharply from 298 to 318 K, while with CRE it was observed to diminish leading to an increase in IE%. The activation parameters without and with CRE in the temperature range of 298–318 K is shown in Table 4. The activation energy (E_a^*) for Al in 1 M HCl was computed from the slope of the graph (Fig. 6) by utilizing the Arrhenius equation:

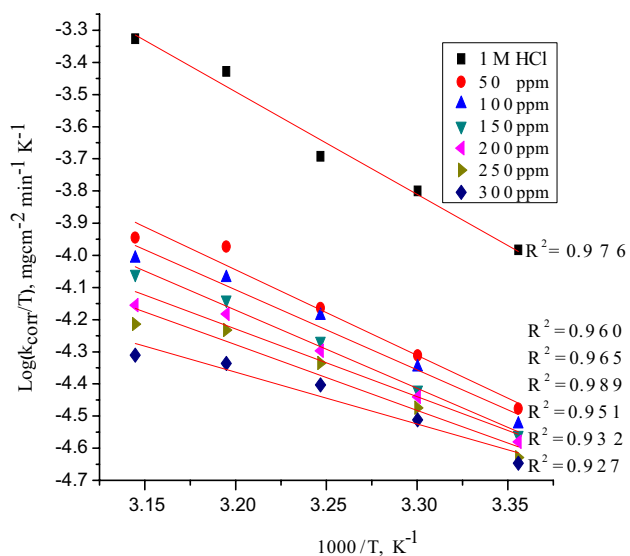$$\log k = -E_a^*/2.303RT + \log A \tag{12}$$
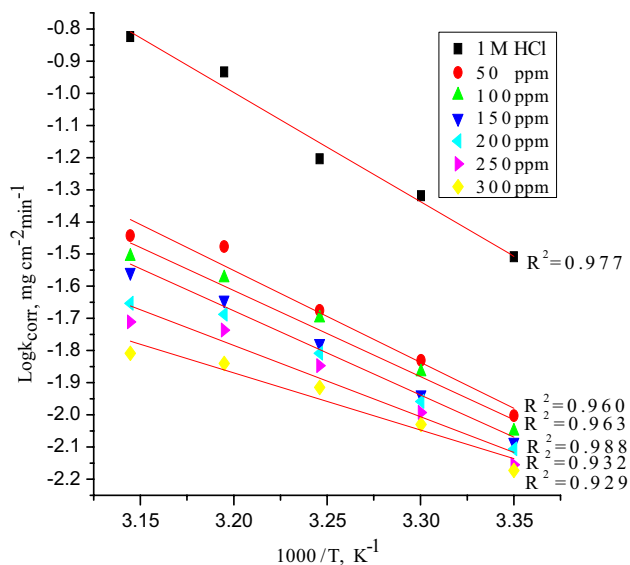
Fig. 6 Arrhenius graph for dissolution rates (k_{corr}) of Al in 1 M HCl (corrosive solution) with and without various doses of CRE

where k expresses the rate of dissolution, E_a^* expresses the activation energy, R expresses the universal gas constant, T the absolute temperature and A the Arrhenius pre-exponential factor [36]. The estimates of change in entropy (ΔS^*) and change in enthalpy (ΔH^*) can be computed by utilizing the equation (Fig. 7):

$$k_{corr} = \left[RT/Nh \exp(\Delta S^*/R) \exp(-\Delta H^*/RT) \right] \qquad (13)$$

where k expresses the dissolution rate, h the Planck's constant, N the Avogadro number, ΔS^* the entropy of activation

and ΔH^* the enthalpy of activation. The negative values of ΔS^* for the CRE infer that the activated complex in the rate-determining step indicates an association instead of dissociation step, signifying that a lack in disorder occurs starting from the reactants to the activated complex [37]. The negative sign of ΔH^* confirms the exothermic feature of the dissolution process. In general, an exothermic process detects either physical adsorption or chemical adsorption.
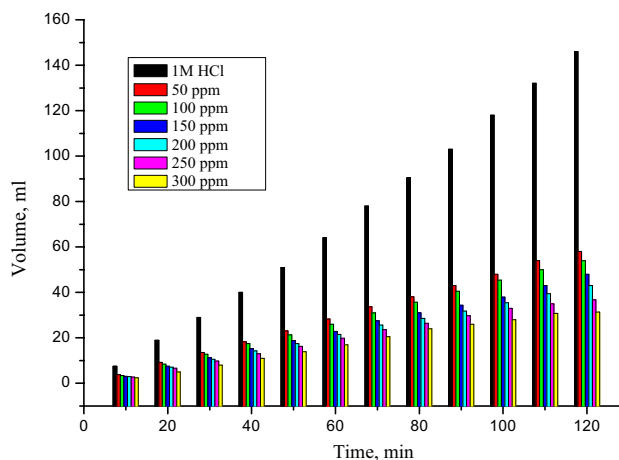
3.2 Hydrogen Evolution Method

Figure 8 shows that there is a linear relationship between the volume of evolved H_2 gas and time. The average of evolved H_2 gas is limited at the start of the reaction then increases significantly with time. Due to Al being soluble in acidic aqueous medium with the release of hydrogen gas, the amounts of released hydrogen gas are based on the Al dissolution rate which is measured from the slope of the curve in the presence and absence of the inhibited acid solution. Adding CRE limits the rate of evolved H_2 gas with increasing doses. The estimates of %IE of various doses of CRE are summarized in Table 5 [25].

3.3 Acidification Method

In this acidimetric method, the corrosion reaction of the metal was monitored as a function of the change of [H^+] in the acid solution. The equation for the corrosion of Al metal in dilute HCl solution can be represented thus:

$$Fe + 2HCl === FeCl_2 + H_2 \qquad (14)$$
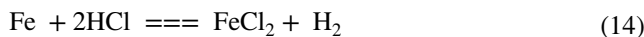
The H_2 may dissolve and affect the measured value of the pH. It must, however, be considered that factors which

Fig. 7 Plot of log (k_{corr}/T) against ($1000/T$) of Al in 1 M HCl (corrosive solution) with and without different doses of CRE

Fig. 8 Variation of the volume of H_2 gas evolved versus time for Al dissolution in 1 M HCl (corrosive solution) with and without different doses of CRE at 298 K

Table 5 Computed values of CR and %IE for Al dissolution in 1 M HCl (corrosive solution) including CRE at 298 K from the H_2 evolution method at 120 min

Conc. (ppm)	Corrosion rate (ml/min)$\times 10^4$	%IE
Blank	12,166	–
50	4633	61.9
100	4500	63.0
150	3750	69.2
200	3583	70.5
250	3066	74.8
300	2616	78.5

affect the acidity of a salt solution are mainly size, charge density of the cation, and the nature of the solution. Ions of small size and high charge easily hydrolyse to yield considerable amounts of H^+ in aqueous solution to affect acidity, with Fe^{3+} and Al^{3+} being good examples [38]. The aqueous solution of $AlCl_3$ in acidic medium is always clear because the hydrolysis of $AlCl_3$ will not be significant enough to alter the H^+ level to make the results unreliable. Also, in an acidic solution like this medium, the equilibrium in Eq. (15) shifts more to the left-hand side and therefore the $[H^+]$ will be significantly low.

$$Al^{3+} + HOH ==== [Al\ OH]^{2+} + H^+ \qquad (15)$$

This is why an aqueous solution of $AlCl_3$ in acidic medium is always clear. The corrosion rate as observed, i.e. $[H^+]$ (Table 6), decreased with the increase in the concentration of the extract and hence the increase in %IE. This is a clear propensity of inhibitive action of the extract for the corrosion of the Al sample in the acid medium [39]. The same trend was observed in the case of the gravimetric method (Table 2). These two techniques gave very comparable results of (%IE). This suggests that the acidimetric technique can be conveniently adopted for corrosion inhibition evaluation. However, values obtained through the acidimetric technique are slightly higher than those of the gravimetric technique. As earlier pointed out, the possibilities of

Table 6 Values of %IE for the acidimetric method for CRE at 298 K

| Conc. (ppm)	$[\Delta H^+]\times 10^4$	θ	%IE
Blank	90.4	–	–
50	22.3	0.753	75.3
100	21.7	0.760	76.0
150	20.3	0.775	77.5
200	19.8	0.781	78.1
250	18.5	0.795	79.5
300	16.5	0.817	81.7

the introduction of errors into the results are greater in the gravimetric technique than in the acidimetric method.

3.4 Tafel Extrapolation Curves

Tafel extrapolation curves for the corrosion of Al were studied to examine the type of the inhibitor. The dissolution rate and dissolution current density (i_{corr}) of Al in the bare solution diminishes by adding CRE. The presence of the CRE raises both the cathodic and anodic overvoltages and raises the shift in their values to the more negative and positive. The analogous cathodic and anodic Tafel curves in Fig. 9 confirm that the reduction and dissolution mechanisms experienced no change in the presence of CRE [40]. Thus, it can be deduced that CRE is considered as mixed-type inhibitor adsorbed on the cathodic locations of Al and which diminishes the evolution of hydrogen gas. Further, the molecules of CRE adsorbed on anodic locations diminish the anodic dissolution of Al [41]. Values of E_{corr} slightly shift in a trend of less negative. Tafel slopes do not change and the E_{corr} shift is less than 85 mV, confirming mixed-type inhibitor (Table 7).

3.5 EIS Tests

EIS is a non-ruinous technique on the interface between the electrode and the corrosive solution. The protection quality (%IE) can be computed by R_{ct} due to the formation of the protective layer on the Al surface. Among its advantages is an ability to compute R_{ct} and C_{dl} by utilizing the amplitude to decrease the error of the measurements. This is an Impedance technique and the resistance increases by increasing the dose of CRE, Impedance is the power of measuring the
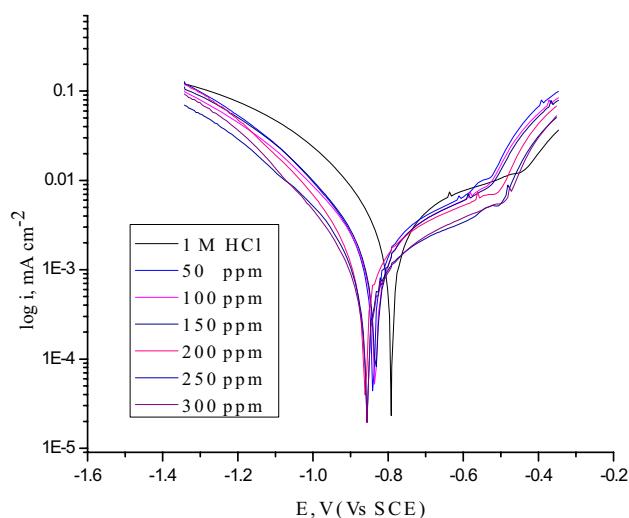
Fig. 9 Tafel extrapolation curves for the dissolution of Al in 1 M HCl (corrosive solution) with and without different doses of CRE at 298 K

Table 7 Effect of CRE doses on the electrochemical dissolution parameters of Al in 1 M HCl (corrosive solution) at 298 K

Conc. (ppm)	$-E_{corr}$ (mV vs. SCE)	i_{corr} (mA cm^{-2})	β_a (mV dec^{-1})	$-\beta_c$ (mV dec^{-1})	C.R (mpy)	θ	%IE
Blank	791	16.1	265	303	629.0	–	–
50	713	2.4	234	254	93.5	0.851	85.1
100	716	1.69	232	236	66.0	0.895	89.5
150	736	1.65	260	260	64.5	0.899	89.7
200	730	1.03	290	199	40.0	0.936	93.6
250	736	0.511	237	241	20.0	0.96.8	96.8
300	729	0.408	244	179	15.5	97.5	97.5

resistance of a circle to the current flow. Impedance estimates occur by implementing the AC potential and quantifying the current passed within the cell. R_{ct} can be measured from the Bode plots by taking a tangent to the Y-axis at high frequency ($R_{ct} + R_S$) and taking a tangent for *the X*-axis at low frequency (R_{ct}) and subtracting from each other, resulting in R_{ct}. %IE can be computed from the equation:

$$\%IE = \left[1 - \left(R'_{ct}/R_{ct}\right)\right] \times 100 \qquad (16)$$

Then R'_{ct} and R_{ct} are the charge transfer resistances of 1 M HCl (corrosive solution) and CRE, respectively.

The Nyquist plot, C_{dl}, which is the relationship between Z_{imag} and Z_{real}, can be estimated by computing R_{ct}, which is the diameter of the high-frequency loop and, owing to C_{dl}, is inversely proportional to the R_{ct}; C_{dl} can be computed from the equation:

$$C_{dl} = \frac{1}{2\pi f_{max} R_{ct}} \qquad (17)$$

Nyquist impedance Fig. 10 spectra do not exhibit ideal semicircles [42] due to C_{dl} roughness and the electrode surface heterogeneity. R_{ct} increases by increasing the dose of the examined CRE, so that there is a decline in the dissolution rate. C_{dl} values diminish with the CRE dose increasing, which is associated with the progressive replacement of water molecules in the double layer by the adsorbed extract particles, diminishing the dielectric constant of the metal solution interface, increasing the thickness of the double layer and diminishing the trend of the dissolution reaction [43]. The experimental data of Nyquist graphs can be determined by using the circuit in Fig. 11, in which R_{ct} represents the charge-transfer resistance, R_s represents the electrolyte resistance and the constant phase element. The inhibition behavior of the inhibitor resulting from other procedures was confirmed by the impedance data (Table 8).

3.6 EFM Tests

EFM is a rapid and non-ruinous technique, which draws a relationship between current and frequency without knowing the Tafel constants (Fig. 12). It gives information about (i_{corr}) immediately, thus differing from the polarization technique. The height [44] of the peaks is a measure for (i_{corr}) and which is a measure of protection quality %IE. In this technique, frequency is implemented and (i_{corr}) is measured. EFM is a non-linear response at which (i_{corr}) diminishes in going towards doses of CRE, owing to (i_{corr}) being the current resulting from dissolution and so in the case of CRE should have small values. In this technique, we insert a current higher than what should be inserted due to not needing to make the polarization in Table 9 change slightly confirming that CRE is a mixed-type inhibitor. Causality factors [45] (CF-2 and CF-3) make internal checks on the validity of the estimates, and their values of around 2 and 3 are evidence for the validity of the results. The electrochemical parameters were detected and are set out in Table 9.

3.7 ATR-FTIR and UV/Visible Spectral Analysis

Figure 13 shows the relevant ATR-FTIR spectra.

3.7.1 ART-IR Analysis

This analysis shows that there are two peaks, at 641 cm^{-1} and 677 cm^{-1}, referring to the SO$_4^{2-}$ group, a peak at 710 cm^{-1} referring to skeletal C–C vibrations, a peak at 986 cm^{-1} referring to vinyl (=C–H)/aromatic C–H in plane bend, a peak at 1105 cm^{-1} referring to C–C of alkane/C=S thio carbonyl, a peak at 1227 cm^{-1} referring to sulfate ester (C–O stretch), a peak at 1398 cm^{-1} referring to carboxylic acid salt/phenol//tertiary alcohol///ammonium ions, a peak at 1644 cm^{-1} referring to alkene (C=C)/(C–O) of amide CONH$_2$//conjugated ketone, a peak at 2071 cm^{-1} referring to the isothiocyanate (–NCS group)/cumulated system (C=C=O)//transition metal carbonyl, a peak at 2812 cm^{-1} referring to the C–H stretch, two peaks at 3239 cm^{-1} and 3523 cm^{-1} referring to alcoholic O–H, and a very weak peak at 3804 cm^{-1} referring to the crystallization of water [46, 47].

Fig. 10 EIS Nyquist plots (**a**) and Bode plots (**b**) of Al in 1 M HCl (corrosive solution) with and without different doses of CRE at 298 K
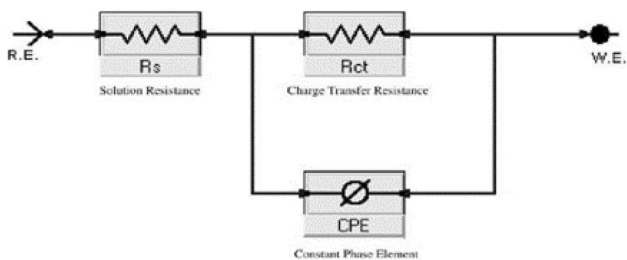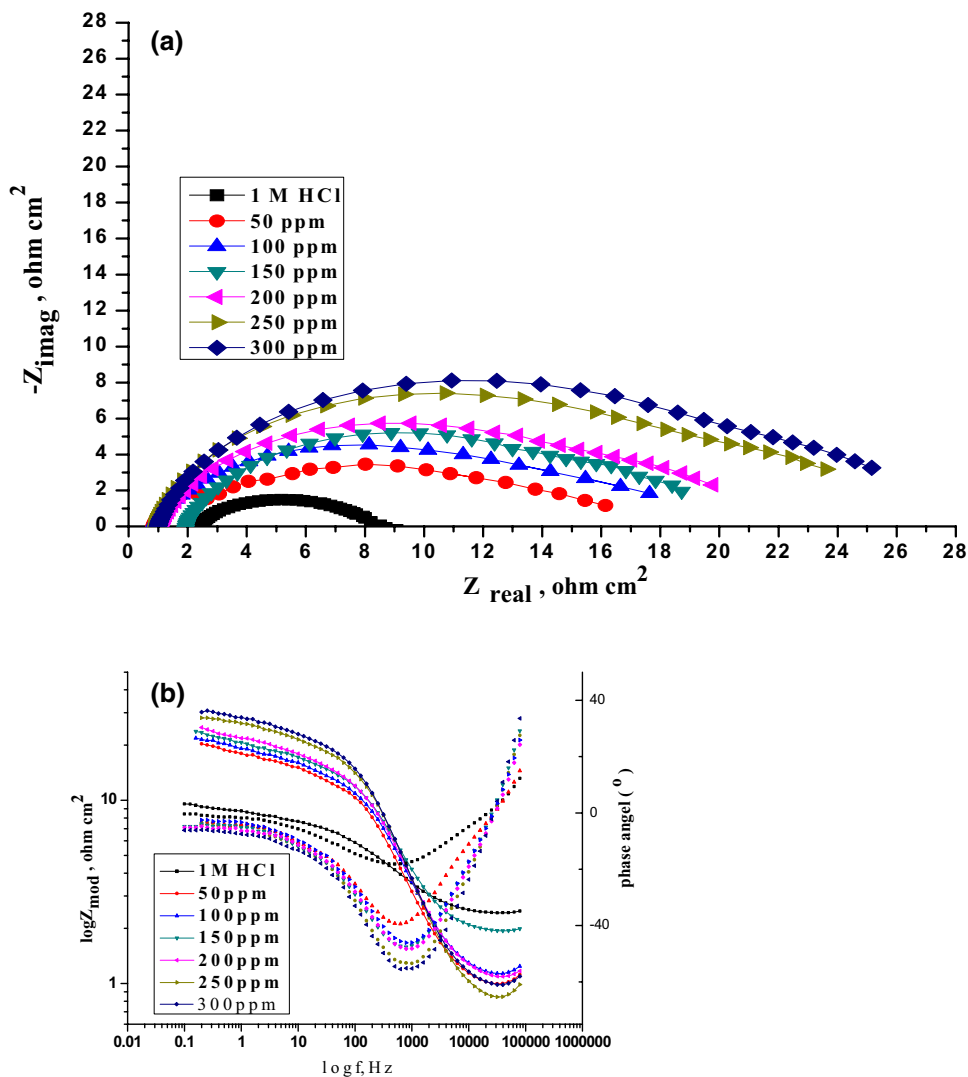
Fig. 11 Electrical equivalent circuit model used to fit the results of impedance

Table 8 EIS parameters for the dissolution of Al in 1 M HCl (corrosive solution) with and without different doses of CRE at 298 K

Conc. (ppm)	$C_{dl} \times 10^5$ (F cm^{-2})	R_{ct} (Ω cm^2)	θ	%IE
Blank	438	5.44	–	–
50	5.5964	23.23	0.766	76.6
100	3.7042	33.51	0.838	83.8
150	3.4877	40.16	0.864	86.4
200	3.3273	67.62	0.920	92.0
250	2.5008	90.49	0.940	94.0
300	1.8277	128.40	0.958	95.8

3.7.2 ATR-IR Analysis

This analysis shows a shift of (C=C)/(C–O) of the amide// conjugated ketone from 1644 to 1650 cm^{-1}, a shift of alcoholic O–H from 3239 and 3523 to 3381 cm^{-1}, confirming the adsorption of inhibitor molecules. There is a disappearance of peaks at 986 cm^{-1}, 1105 cm^{-1}, 1227 cm^{-1}, 2071 cm^{-1}, and 2812 cm^{-1}, and three new bonds of the aromatic nitro group formed at 1520 cm^{-1}, 1541 cm^{-1}, and 1558 cm^{-1} (N–O stretch) (Fig. 13).
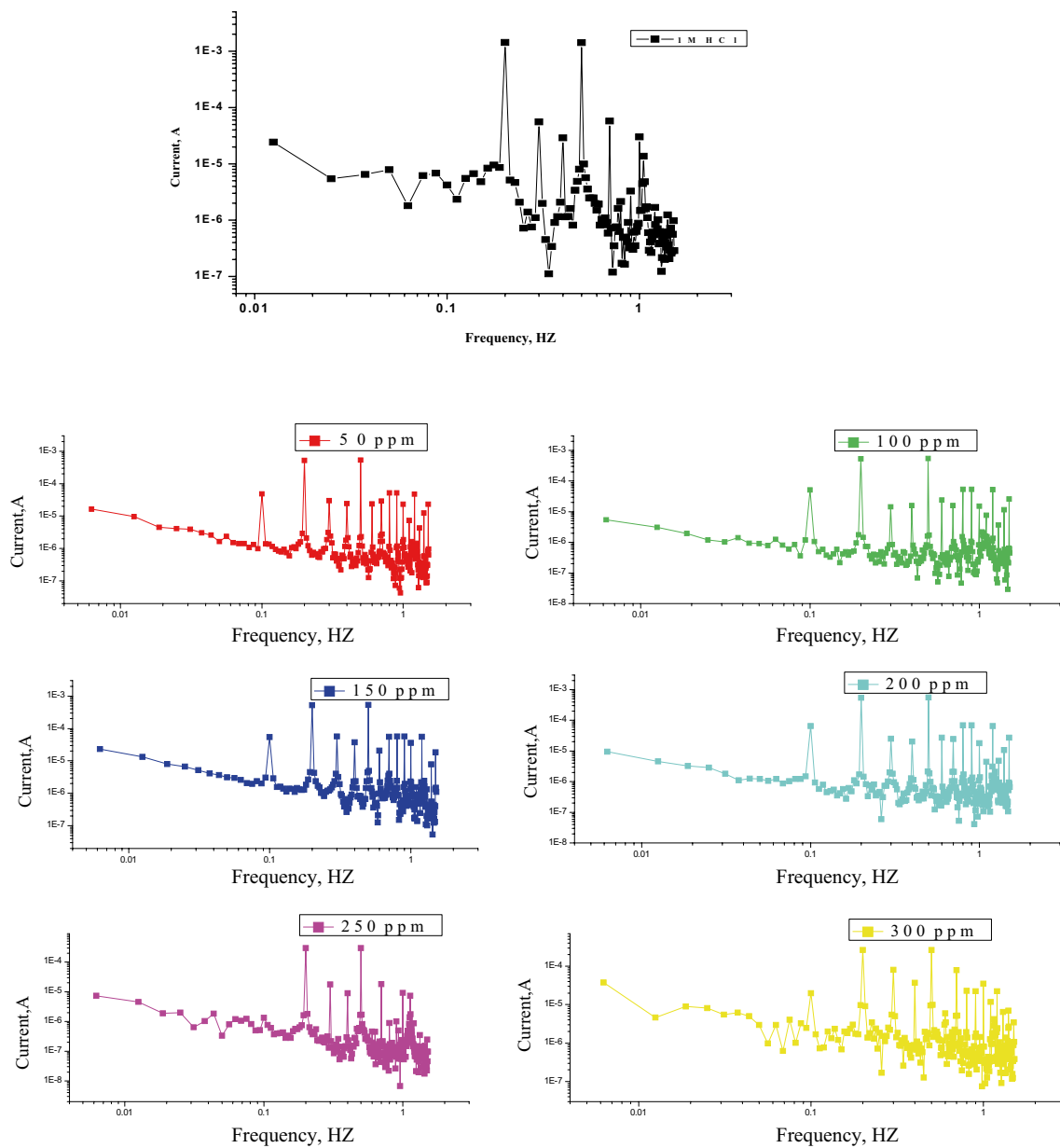
Fig. 12 EFM spectra of Al dipped in solutions of 1 M HCl (corrosive solution) treated with different doses of CRE at 298 K

Table 9 EFM data for the dissolution of Al in 1 M HCl (corrosive solution) containing different doses of CRE at 298 K

Conc. (ppm)	i_{corr} (μAc m^{-2})	β_a (mV dec^{-1})	$-\beta_c$ (mV dec^{-1})	CF-2	CF-3	C.R (mpy)	θ	%IE
Blank	672.5	223	192	1.9	2.3	262.0	–	–
50	363.2	50	52	1.8	1.4	141.4	0.460	46.0
100	305.3	33	41	1.9	2.5	119.0	0.546	54.6
150	285.9	29	39	1.9	2.5	111.4	0.575	57.5
200	164.5	25	64	1.9	2.1	64.1	0.755	75.5
250	161.1	29	48	1.9	2.7	62.8	0.760	76.0
300	154.7	39	60	1.9	2.0	60.5	0.770	77.0

Fig. 13 **a** Al ATR-FTIR spectra after dipping in 1 M HCl (corrosive solution) + 300 ppm of CRE, **b** pure CRE before immersion
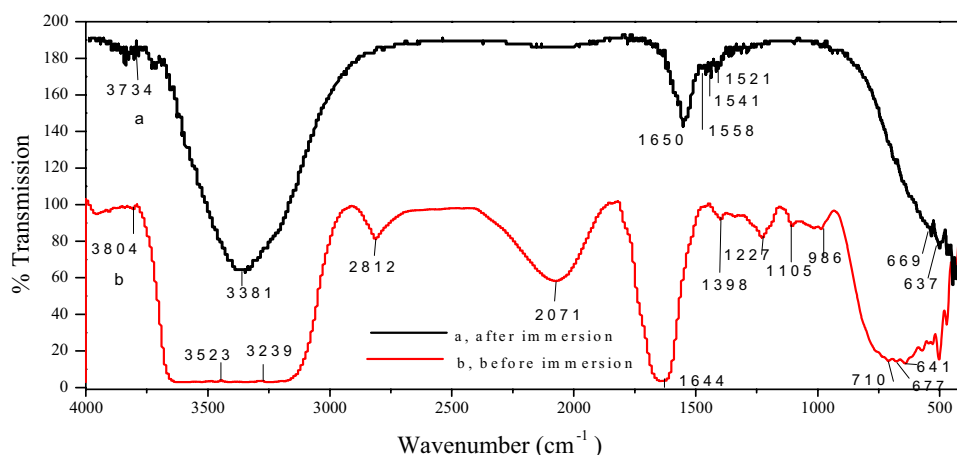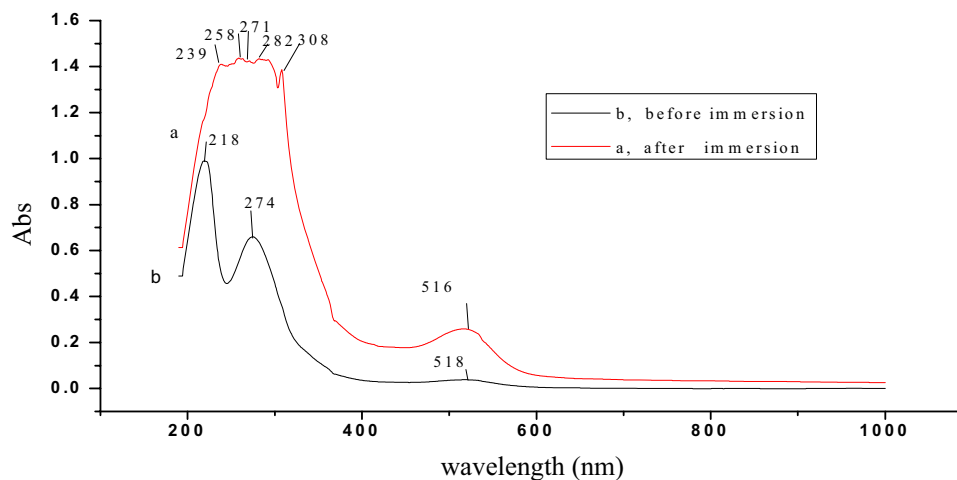
3.7.3 UV Spectroscopy

Figure 14 shows the relevant UV/Vis spectra.

3.7.3.1 Before Immersion The value of 518 nm refers to the polyene system β-carotene, 274 nm to β-carotene (–C–CH=CH–C–)/NR_2 polar group//tyrosine, and 218 nm to the peptide bond/R–S–R system//acyclic ketone///parent open chain or heteroannular diene or cyclo hexane [48].

3.7.3.2 After Immersion The value 516 nm refers to the polyene system β-carotene, 308 nm to the phenyl structure benzenonitrile, 282 nm to the formation of –C=N–NH–C=S –NH_2/aniline, 271 nm to the diene –NR_2 polar group, 258 nm to guano sine/phenyl alanine $C_9H_{11}NO_2$, and 239 nm to the R2S/peptide bond (R-HC-CONH-CH-R)//aniline 'protein///H_2C = CH-CH_2-CH=NOH////R– CO–NH–CO–R. There are five bands after immersion which means that new bands also formed demonstrating that IR results confirmed adsorption (Fig. 13).

3.8 AFM Studies

AFM provides images from which it is possible to compute the roughness of metal superficies. The three-dimensional and two-dimensional AFM micrographs for the Al surface in 1 M HCl (bare solution) with and without CRE are shown in Fig. 15, the data inferring that the Al surface dipped in 1 M HCl (bare solution) overnight is higher in surface roughness than the inhibited Al, which reveals that the Al sample is acutely deteriorated due to the corrosive medium. The average roughness of the protected Al was diminished to 437.2 nm (Table 10) and these parameters reveal that the surface is soft. The softness of the surface is due to the setting up of a condensed protective film of the CRE on the metal surface, hence protecting the Al surface deterioration.

3.9 Biological Activity

The results of Table 11 show that CRE has a good impact against bacterial growth, so that the corrosion rate is diminished.

Fig. 14 UV/visible spectra of CRE solution (a) and the corrosive solution containing CRE after immersion of Al coupons for 24 h (b)

Fig. 15 Three-dimensional AFM images of the polished surface of Al dipped in 1 M HCl and in 1 M HCl containing 300 ppm of the extract

Sample	(3D)	(2D)
Blank		
300 ppm extract		
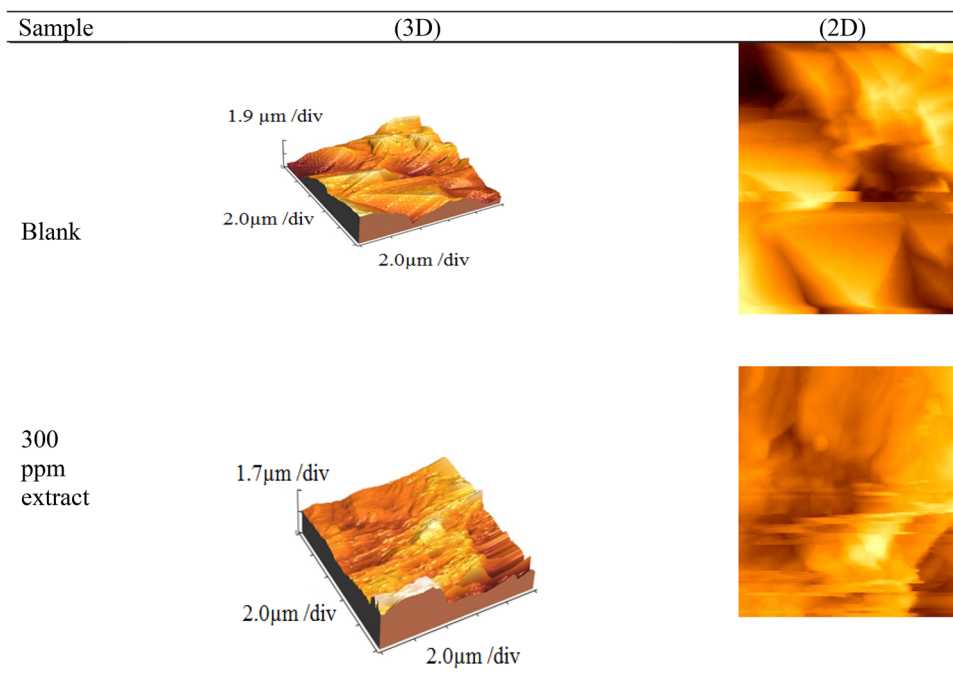
Table 10 AFM estimations for Al surface in the presence and absence of CRE
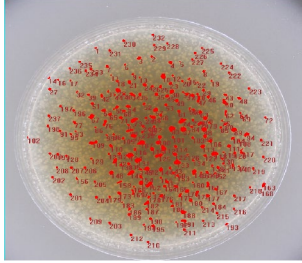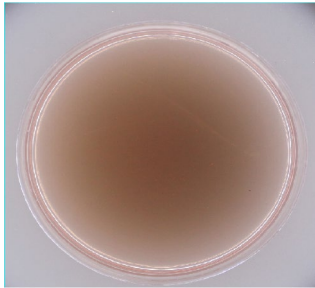
Sample	Ave rough (R_a) nm	R_{ms} rough nm (R_q)	The peak valley height (R_p) μm
Blank	667.1	825.0	2.910
Cerumium rubrum	437.2	573.3	2.139

R_{ms} rough (root-mean-squared roughness)

(R_q), Ave rough (average roughness), R_a

R_p = peak valley height

Table 11 Bacteria colonies cultivated in Petri dishes computed by the Doc-it colony counter device for blanks of bacteria compared with pure and 300 ppm of CRE

No. of colonies	Counting by Doc it colony device
Blank number. of colonies is 241	
Pure and 300 ppm CRE: the same result of 0 colony	

4 Conclusions

1. *Cerumium rubrum* (CRE) acts as good inhibitor to protect Al against dissolution in corrosive solutions.
2. The data collected from chemical methods (WL method, hydrogen evolution, acidification method) and electrochemical (potentiodynamic polarization, EIS, and EFM) techniques reveal that the protection quality relies on the dosage of the investigated CRE and the temperature of the corrosive solution, meaning that it increases with increasing CRE doses, and solution temperature
3. The adsorption of the inspected CRE on the Al surface in 1 M HCl (corrosive solution) matches the Langmuir adsorption isotherm
4. The thermodynamic parameters acquired by this research indicate that the activation energy diminishes in the presence of CRE and the negative values of ΔG_{ads}° indicates that the adsorption is irreversible
5. C_{dl} diminishes with regard to the case of the free acid when the CRE is present in the corrosive solutions, which can be ascribed to the adsorbed molecules.

6. CRE molecules established a covering film through either the possibility of sharing free electrons on the hetero-atoms or π–electron interaction of the aromatic nucleus.

References

1. Kasuga B, Park E, Machunda RL (2018) Inhibition of Al corrosion using carica papaya leaves extract in sulphuric acid. JMMCE 6:1–14
2. Raghavendra N, Bhat JI (2018) Protection of Al metal in 0.5 M HCl environment by mature arecanut seed extracts: a comparative study by chemical, electrochemical and surface probe screening techniques. J Phys Sci 29(1):77–99
3. Narasimha R, Jathi IB (2018) Red arecanut seed extract as a sustainable corrosion inhibitor for Al submerged in acidic corrodent: an experimental approach towards zero environmental impact. Period Polytech Chem Eng 62(3):351–358
4. Raghavendra N, Hublikar LV, Patil SM, Ganiger PJ, Bhinge AS (2019) Efficiency of sapota leaf extract against Al corrosion in a 3 M sodium hydroxide hostile fluid atmosphere: a green and sustainable approach. Bull Mater Sci 42(226):1–11
5. Fouda AS, Etaiw SH, Hammouda M (2017) Corrosion Inhibition of Al in 1 M H_2SO_4 by Tacoma non-aqueous extract. J Bio Tribo-Corros 3(3):3–29
6. Abakedi OU (2017) Al corrosion inhibition by Microdesmis puberula leaf extract in 2 M HCl solution. Int J Inno Sci Eng Tech Res 5(3):6–14
7. Mary AC, Suruthi KS (2018) Chrysanthemum flower extract as a green inhibitor for Al corrosion in alkaline medium. Int J Chemtech Res 11(7):37–44
8. Abdel-Gawad SA, Osman WM, Fekry AM (2019) Characterization and corrosion behavior of anodized Al alloys for military industries applications in artificial seawater. Surf Interfaces 14:314–323
9. Abdel-Gawad SA, Osman WM, Fekry AM (2019) A development of novel Ni-P coating on anodized Al alloys for military industries applications in artificial sea water. Surf Eng 35(12):1033–1041
10. Ghoneim AA, Ameer MA, Fekry AM (2012) electrochemical behavior of Al-Si alloy in phosphoric acid containing halogen or oxyhalogen anions. Int J Electrochem Sci 7(7):10851–10864
11. Raghavendra N, Bhat JI (2018) Anti-corrosion properties of areca palm leaf extract on Al in 0.5 M HCl environment. S Afr J Chem 71:30–38
12. Ennouri A, Lamiri A, Essahli M (2017) Corrosion inhibition of aluminum in acidic media by different extracts of *Trigonellafoenum graecum* L. seeds. Port Electrochim Acta 35(5):279–295
13. Olawale O, Ogundipe BJO, Julius S, Abayomi ST (2018) Optimization and modeling of Al corrosion inhibition using almond (*Prunus amydgdalus*) fruit leaves extract as green inhibitor in HCl acidic medium. IJMET 9(13):1274–1285
14. James AO, Akaranta O (2009) Corrosion inhibition of aluminum in 2.0 M hydrochloric acid solution by the acetone extract of red onion skin. Afr J Pure Appl Chem 3(12):262–268
15. El-Azaly AM (2019) Influence of soybean (glycine max) plant extract on corrosion of Al in 1M HCl. Int J Electrochem Sci 14:2714–2731
16. Imane H, Mohamed E, Abdeslam L (2019) Inhibition of aluminum corrosion in 0.1 M Na_2CO_3 by *Mentha pulegium*. Port Electrochim Acta 37(6):335–344
17. Kumar M, Shankar U (2012) Evaluation of mechanical properties of Al alloy 6061—glass particulates reinforced metal matrix composites. IJMER 2(5):3207–3209
18. Cochran JF, Mapother DE (1958) Superconducting transition in Al. Phys Rev 111:132–142
19. Eladio L, Guillen V (2011) Prospective of the Al industry in venezuela and its role in building sustainable future. Ecodiseno & sostinibilidad 3(1):175–191
20. Polmear IJ (1995) Light alloys: metallurgy of the light metals. 3rd edition. Butterworth-Heinemann, Oxford, pp 1–362.
21. Singh K, Agrawal KK, Mishra V, Mubeen US, Shokla A (2012) A review on: *Thevetia peruviana*. Int Res J Pharm 3(4):74–77
22. Cortés Y, Hormazabal E, Leal H, Urzua A, Mutis A, Parra L, Quiroz A (2014) Novel antimicrobial activity of a dichloromethane extract obtained from red seaweed *Ceramium rubrum* (Hudson) (Rhodophyta: Florideophyceae) against *Yersinia ruckeri* and *Saprolegnia parasitica*, agents that cause diseases in salmonids. Electron J Biotechn 23:126–131
23. IvanovaI V, Stancheva M, Merdzhanova A (2012) Fatty acids composition of macroalgae from Bulgarian Black Sea coast. OUAESS 23(1):35–40
24. Pirjol BN, Pirjol TN, Paraschiv G, Bratu M, Sirbu R, Roncea F, Meghea A (2011) Physical-chemical characterization of some green and red macrophyte algae from the Romanian black sea littoral. Sci Study Res 12(2):173–184
25. Pirjol BN, Pirjol TN, Nastac M, Resteanu A, Sirbu R, Ghassoub R (2009) The marine biomass from black sea coast, composition and characteristics, as an unconventional resource. In European Region Annual Conference Paris-Malmaison, France AAPG pp 103–106
26. Fouda AS, Abo-Shohba R, Hussien WM, Ahmed ES (2015) Chemical and electrochemical study on the effectively of *Melilotus officinalis* extract as save corrosion inhibitor for Al in 1 M hydrochloric acid solutions. Glob J Res Eng 15(3):9–24
27. Song G, Atrens A, Stjohn D (2001) Hydrogen evolution method for the estimation of the corrosion rate of magnesium alloys. In: Mathaudhu SN, Luo AA, Neelameggham NR, Nyberg EA, Sillekens WH (eds) Essential readings in magnesium technology. Springer, Cham, pp 565–572
28. Ating EI, Umoren SA, Udousoro II, Ebenso EE, Udoh AP (2010) Leaves extract of *Ananas sativum* as green corrosion inhibitor for Al in hydrochloric acid solutions. Green Chem Lett Rev 3(2):61–68
29. Adejo SO, Yiase SG, Leke L, Onuche M, Atondo MV, Uzah TT (2019) Corrosion studies of mild steel in sulphuric acid medium by acidimetric method. Int J Corros Scale Inhib 8(1):50–61
30. Fouda AS, Rashwan SM, Mohammed AE, Ibrahim AM (2017) *Salicornia begolovi* as eco-friendly corrosion inhibitor for Al in hydrochloric acid solution. Egypt J Chem 60(4):491–505
31. Nithya A, Shanthy P, Vijaya N, Rathish RJ, Prabha SS, Joany RM, Rajendran S (2015) Inhibition of corrosion of Al by an aqueous extract of Beetroot (Betanin). Int J Nano Corr Sci Eng 2(1):1–11
32. Fouda AS, El-Taweel FM, Elgamil M (2017) Corrosion inhibition of Al in hydrochloric acid solution using some pyrazolocarbothioamide derivatives. Int J Electrochem Sci 12:11397–11418
33. Nnaji N, Nwaji N, Mack J, Nyokong T (2019) Corrosion resistance of aluminum against activation: impact of benzothiazole-substituted gallium phthalocyanine. Molecules 24(207):1–22
34. Fares MM, Maayta AK, Al-Qudah MM (2012) Pectin as promising green corrosion inhibitor of Al in hydrochloric acid solution. Corros Sci 60:112–117
35. Khadraoui A, Khalifa A, Hachama K, Mehdaoui R (2016) *Thymus algeriensis* extract as a new eco-friendly corrosion inhibitor for 2024 Al alloy in 1 M HCl medium. J Mol Liq 214:293–297

36. Abiola KO, Tobunb Y (2010) *Cocos nucifera* L. water as green corrosion inhibitor for acid corrosion of Al in HCl solution. Chin Chem Lett 21(12):1449–1452

37. Li X, Deng S (2012) Inhibition effect of *Dendrocalamus brandisii* leaves extract on Al in HCl and H_3PO_4 solutions. Corros Sci 65:299–308

38. Silvère DY, Valery BK, Guy-Richard KM, Augustin O, Albert T (2018) Cefadroxil drug as corrosion inhibitor for Al in 1 M HCl medium: experimental and theoretical studies. JAC 11(4):24–36

39. Ashassi-S H, Shabani B, Aligholipour B, Seifzadeh D (2006) The effect of some Schiff base on the corrosion of Al in HCl solution. Appl Surf Sci 252:4039–4047

40. El-Haddad MN, Fouda AS (2015) Electroanalytical, quantum and surface characterization studies on imidazole derivatives as corrosion inhibitors for aluminum in acidic media. J Mol Liq 209:480–486

41. Villamizar-Suarez W, Malo JM, Matinez-Villafane A, Chacon-Nava JG (2011) Evaluation of corrosion inhibitors performance using real-time monitoring methods. J Appl Electrochem 41:1269–1278

42. Silberberg MS (2000) Chemistry: the molecular nature of matter and change. 2nd ed, McGraw-Hill, Pennsylvania, pp 785–788.

43. Rajendran A, Karthikeyan C (2012) The inhibitive effect of extract of flowers of *Cassia auriculata* in 2 M HCl on the corrosion of Al and mild steel. J Plant Res 2(1):9–14

44. Arukalam IO, Ijomah NT, Nwanonenyi SC, Obasi HC, Aharanwa BC, Anyanwu PI (2014) Studies on acid corrosion of Al by a naturally occurring polymer (*Xanthan gum*). IJSER 5(3):663–673

45. Nithya A, Shanthy P, Vijaya N, Joseph RR, Santhana PS, Joany RM, Rajendran S (2015) Inhibition of corrosion of Al by an aqueous extract of beetroot (Betanin). Int J Nano Corr Sci Eng 2(1):1–11

46. Singh A, Ahmad I, Quraishi MA (2016) Piper longum extract as green corrosion inhibitor for aluminum in NaOH solution. Arab J Chem 9:S1584–S1589

47. Bosch RW, Hubrecht J, Bogaerts WF, Syrett BC (2001) Electrochemical frequency modulation: a new electrochemical technique for on-line corrosion. Corrosion 57(1):60–70

48. Kumar S (2006) Organic chemistry, spectroscopy of organic compounds. Guru Nanak Dev University, Amritsar, pp 1–36

Publisher's Note Springer Nature remains neutral with regard to jurisdictional claims in published maps and institutional affiliations.